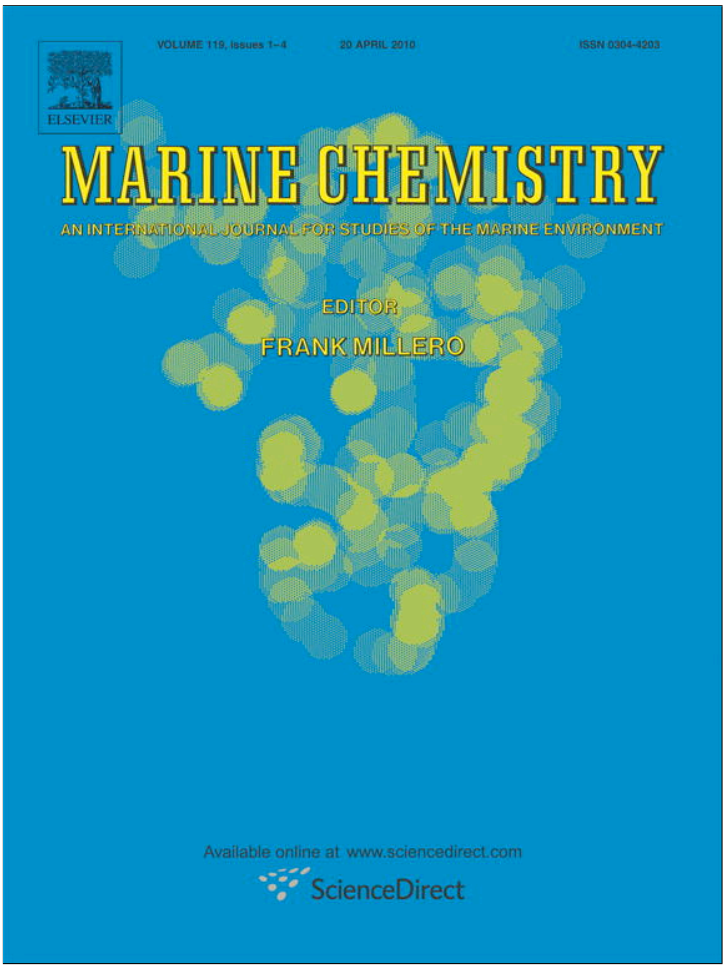

Marine Chemistry 119 (2010) 65–76

Contents lists available at ScienceDirect

Marine Chemistry

journal homepage: www.elsevier.com/locate/marchem

Analysis of dissolved iron isotopes in seawater

Seth G. John *, Jess F. Adkins

California Institute of Technology, Division of Geological and Planetary, Sciences, Pasadena, CA 91125, USA

ARTICLE INFO

Article history:
Received 22 July 2009
Received in revised form 22 December 2009
Accepted 5 January 2010
Available online 18 January 2010

Keywords:
Iron
Iron isotopes
Mass spectrometry
ICPMS

ABSTRACT

Iron is an important nutrient in the ocean. Measuring the stable isotopes of dissolved Fe in seawater may help to answer important biogeochemical questions such as what are the sources and sinks for Fe to the oceans, and how is Fe biologically cycled. Because Fe concentrations in seawater are very low, typically less than 1 nM, there are significant challenges both to separate and purify Fe from seawater without introducing contamination, and to accurately analyze δ^{56}Fe on the small quantities of Fe extracted. New techniques are presented here for separation and purification of Fe from seawater by bulk extraction onto a resin with NTA functional groups, followed by anion exchange chromatography. This method recovers 89% of the Fe from 1 L samples of seawater without causing any fractionation of Fe isotopes, with a total blank of 1.1 ± 0.6 ng Fe. To optimize the analytical procedure for small amounts of Fe, the different sources of error in measurement of δ^{56}Fe have been analyzed. For 252 individual analyses of standards and samples, the internal error is well described by the combination of errors from electronic noise on the detectors (Johnson noise), counting statistics, and a third source of error hypothesized to be short-timescale flicker in instrumental mass bias. With the small amounts of iron found in natural seawater samples, error is dominated by Johnson noise and counting statistics. Our analyses also include 160 pairs of "intermediate" replicates in which the same post-purification sample was measured during different analytical sessions, and 141 pairs of "external" replicate analyses for samples prepared from the same original seawater carboy but which were extracted and purified separately. The portion of overall mass spectrometry error that derives from intermediate error has been evaluated by comparing the variance in δ^{56}Fe for a single sample measured during multiple analytical sessions with the internal variance in δ^{56}Fe for the multiple cycles of data that make up each single analysis. The portion of total external error that derives from internal error was determined from variance in δ^{56}Fe for external replicates, compared with internal error based on the variance in cycles for each single analysis. We find that the error for multiple analyses of a sample during different analytical sessions is 1.06 times the internal error, and the external error for analysis of Fe samples which have been separately purified and extracted from the same original seawater is 1.26 times the internal analytical error. Based on this error analysis, we suggest that dissolved Fe isotopes in seawater are best measured by separately extracting the Fe from a single liter of seawater and measuring the entire quantity of extracted Fe in a single short analysis. Using this method, the predicted accuracy for measurements of seawater dissolved δ^{56}Fe ranges from 0.2‰ to 0.05‰ (2σ) for seawater Fe concentrations of 0.1 nM and 1.0 nM, respectively.

1. Introduction

Many natural marine processes fractionate iron (Fe) isotopes, suggesting great promise for seawater δ^{56}Fe as a new tracer for Fe biogeochemical cycling. There is only a small range in δ^{56}Fe of most silicate rocks and for loess and aerosols of the sort that might be deposited into the surface ocean, generally between 0‰ and +0.2‰ (Beard et al., 2003; Dauphas and Rouxel, 2006; de Jong et al., 2007). The chemical cycling of Fe in the oceans, however, can lead to large δ^{56}Fe signatures which are easily distinguished from bulk earth background. For example, the measured δ^{56}Fe of hydrothermal fluids from a variety of vent-types ranges from −0.67‰ to −0.09‰ hydrothermal sulfide δ^{56}Fe measurements range from −2.10‰ to +0.34‰, and δ^{56}Fe values as high as +1.20‰ have been measured in hydrothermal plume particulates (Beard et al., 2003; Rouxel et al., 2008a; Severmann et al., 2004; Sharma et al., 2001). Comparatively negative δ^{56}Fe values, from −2.96‰ to −1.3‰ have been measured in anoxic pore waters in marine sediments, where isotopically light Fe (II) is released into solution (Bergquist and Boyle, 2006; Severmann et al., 2006; Staubwasser et al., 2006). Even larger variation has been seen in a subterranean estuary with dissolved δ^{56}Fe isotopes ranging from −4.91‰ to +0.44‰ (Rouxel et al., 2008b). Biological processes such as dissimilatory Fe reduction (Beard et al., 1999; Crosby et al., 2005, 2007) and Fe(II) oxidation (Croal et al., 2004) may fractionate

* Corresponding author.
E-mail address: sjohn@gps.caltech.edu (S.G. John).

0304-4203/$ – see front matter © 2010 Elsevier B.V. All rights reserved.
doi:10.1016/j.marchem.2010.01.001

Fe isotopes in certain marine environments. Abiotic processes such as riverine Fe cycling (Bergquist and Boyle, 2006; Fantle and DePaolo, 2004), ligand-promoted mineral dissolution (Brantley et al., 2004), and mineral precipitation (Bullen et al., 2001) could contribute to an offset between the bulk δ^{56}Fe of riverine and dust particles, and the δ^{56}Fe of dissolved Fe released from these particles. As each of these processes leave their unique imprint upon seawater δ^{56}Fe, the analysis of Fe isotopes in seawater may help us to fingerprint Fe sources to the ocean and to better understand the biological cycling of Fe in the oceans.

Recent studies on the dissolved iron isotope composition of seawater show that seawater δ^{56}Fe can be measured with sufficient accuracy to distinguish natural variability. Lacan et al. (2008) have measured seawater δ^{56}Fe in the Southern Ocean and have discovered significant natural variations. Seawater dissolved δ^{56}Fe was +0.04‰, +0.09‰, −0.13‰, and +0.21‰ at 30 m, 200 m, 1250 m and 4000 m, respectively. With measurement precision of 0.09‰ (2σ SD), these natural variations are considerably greater than analytical uncertainty and probably represent the impact of some subset of the processes described above on the seawater δ^{56}Fe signature. Dissolved iron in the North River estuary has an average δ^{56}Fe of +0.43‰ (Escoube et al., 2009). Finally, we have measured seawater δ^{56}Fe in the San Pedro Basin (δ^{56}Fe = 0‰ to −1.82‰) and the North Atlantic (δ^{56}Fe = +0.3‰ to +0.7‰) and believe that these variations can be interpreted as signatures of the source of Fe to the oceans. Analyses of these samples were used to develop the methods described here.

The accurate measurement of natural δ^{56}Fe has become possible with the development of a new generation of multi-collector ICP-MS instruments that have the ability to separate Fe ions from interferences such as ArO^+, ArN^+, and $ArOH^+$, either optically, using a high resolution mode, or with a collision/reaction cell. Typical errors of better than 0.1‰ for greater than ~1 μg of Fe have been achieved by many groups on different instruments. Dauphas and Rouxel (2006) have reviewed some of the instrumental and methodological developments that make such measurements possible. Measuring Fe isotopes in seawater, however, presents a new set of challenges. One liter of seawater typically contains between 5 ng to 50 ng Fe (0.1–1 nM). Consequently, methods used for extraction and purification of Fe must have a very low blank, and instrumental adjustments must be made to accurately measure δ^{56}Fe on such small samples. De Jong et al. (2007) report a method for co-precipitation of Fe from seawater with $Mg(OH)_2$ for iron isotopic analysis. This method is highly efficient at removing Fe from seawater, but has procedural blanks of ~10 ng Fe per liter of seawater that limit its use to measuring δ^{56}Fe on coastal waters. Lacan et al. (2008) report the use of a resin with NTA functional groups (Lohan et al., 2005) to separate Fe from 10 L seawater samples with a blank of 8 ng Fe. This method provides a substantial improvement in terms of reducing blank contribution, though the requirement for such large samples may make sampling and sample processing difficult and would limit its utility for a large-scale undertaking such as GEOTRACES. Continual improvement of such methods to decrease blank, decrease seawater volume requirements, improve analytical accuracy, and simplify processing will increase the practical utility of seawater δ^{56}Fe as a marine biogeochemical tracer.

The importance of iron in the ocean stems directly from the low concentration of Fe in surface seawater, providing an analytical imperative to measure δ^{56}Fe at low iron concentrations. In this paper, new methods are described for extracting Fe from seawater, and analytical developments to measure δ^{56}Fe when the sample size is small (10–1000 ng) are discussed. We hope these methods will facilitate simpler measurements of seawater δ^{56}Fe, and that these methods will be helpful when measuring stable isotope ratios on other samples when sample size is small.

2. Methods and methods development

2.1. Sample collection

Seawater samples for this study were collected in the San Pedro Basin using Teflon-coated X-Niskin bottles, and in the North Atlantic during the first GEOTRACES Intercalibration cruise using the GEOTRACES rosette. Samples were filtered either through 0.45 μm polyethersulfone membrane filters (San Pedro Basin) or an Osmonics capsule filter (GEOTRACES Intercalibration). After collection, samples were acidified to pH 1.7 or pH 2. Samples were ammended with 10 μM H_2O_2 immediately before Fe extraction. All labware was teflon except for autosampler vials. In our CETAC ASX-100 autosampler, we use 20 mL HDPE scintillation vials (Globe Scientific) instead of the larger teflon standard vials and we use 4 mL polyethylene scintillation vials (Globe Scientific) instead of the smaller teflon standard vials. 2 mL polypropylene microcentrifuge tubes (Globe Scientific) in a custom made sample rack are used for samples. Each new lot of vials is tested before use to ensure that they do not contain Fe. Generally, we have found that plasticware from Globe Scientific is clean for trace metals (also K. Bruland and E. Boyle, pers. comm.) although individual lots have been found to be contaminated with Fe (E. Boyle, pers. comm.). After collection, all samples were manipulated in Class-100 clean conditions (Table 1).

2.2. Iron concentration measurements

Over the course of this research, iron concentrations were measured to test for Fe uptake onto resins and elution of Fe from resins, and to measure final sample [Fe] before isotope analysis. Fe concentrations were calculated using the ICPMS signal intensity on ^{56}Fe and ^{54}Fe with an Agilent 7500, a Finnigan Neptune, or a Finnigan Element I. Because Fe concentrations were typically measured by signal intensity alone, rather than by isotope dilution, any Fe concentration measurements reported here are accurate to within ~5 to10%. Standard additions were used for any samples with unknown matrices to ensure that matrix effects on sensitivity were insignificant.

2.3. Iron extraction from seawater

Fe was extracted from seawater using a bulk-extraction technique with NTA Superflow resin (Qiagen). This resin has successfully been

Table 1
A brief procedural outline for extraction and purification of Fe from seawater for isotopic analysis.

Extraction of Fe from seawater with NTA resin
1. Clean resin by leaching for 1 week in 1% HCl.
2. Add 650 μL pre-cleaned NTA resin to 1 L seawater samples with (pH 1.7 to 2, 10 μM H_2O_2).
3. Shake samples for at least 2 h.
4. Pour sample through filter to separate NTA resin.
5. Rinse NTA resin with 3 × 50 mL 0.1% HCl (pH ~2, 10 μM H_2O_2).
6. Elute Fe from resin in 4 × 2 mL 10% HCl.
7. Resuspend NTA resin in original seawater sample, repeat shaking, rinsing and elution combining the eluent from both extractions into a single sample.
8. Evaporate samples and reconstitute in 200 μL 7 N HCl + 0.001% H_2O_2 for purification by anion exchange chromatography.

Purification by anion-exchange chromatography
1. Add 20 μL pre-cleaned AG-MP1 resin to PTFE micro-columns.
2. Clean resin with 3× ~200 μL 7 N HCl + 0.001% H_2O_2.
3. Rinse resin with 6x ~100 μL 2 N HCl.
4. Condition column with 50 μL 7 N HCl + 0.001% H_2O_2.
5. Add sample.
6. Rinse sample in 6× 50 μL 7 N HCl + 0.001% H_2O_2.
7. Elute Fe in 4× 100 μL 2 N HCl.
8. Evaporate and reconstitute in 0.07 N HNO_3 for isotopic analysis.

used to extract Fe from seawater for concentration analysis by ICP-MS and flow-injection analysis (Lohan et al., 2005, 2006) and for analysis of Fe isotopes (Lacan et al., 2008). While previous methods have extracted Fe onto the NTA resin by column chromatography, we have opted instead to use the resin in a bulk-extraction technique. The advantage of a bulk extraction technique is that a smaller volume of resin is used, which decreases the resin blank. It has also been our personal experience that bulk extraction techniques are faster and easier than column extraction.

The partition coefficient for Fe between seawater and the resin was investigated under a number of different conditions using spiked seawater samples, prepared from natural seawater made Fe-free with NTA resin and subsequently spiked with 2 nM Fe. Because Fe speciation is dominated by inorganic complexes at this pH, we expect that this spiked seawater closely mimics the chemistry of natural Fe in seawater. Over many replicate tests, the partition coefficient for Fe was found to be $K = 3.9 \pm 0.7$ (1σ SD, $n = 9$) where

$$K = \frac{[resin - Fe]}{[resin][Fe]} \quad (1)$$

and the amount of resin in the sample is measured in mL/L. Resin volume in distilled water is approximated by eye after settling in a clear centrifuge tube. Saturation of binding sites on the resin by Fe is assumed to be minimal because the partition coefficient did not change for experiments with Fe concentrations between 1 and 20 nM Fe. The partition coefficient in distilled water is ~100, indicating that there is significant competition for NTA binding sites from other seawater salts. Between pH 1.7 and pH 6.7, we did not find any significant difference in the partition coefficient. At pH 1.4, the partition coefficient in seawater was 2.8 indicating a reduced ability of the resin to bind Fe. We found that the half-time for binding to the resin was 30 min when samples were shaken vigorously enough on a shaker table to keep the resin suspended in the seawater (Fig. 1A). When samples were shaken gently in a manner meant to approximate the motions of a boat at sea the binding half-time was 1.5 h, and the binding half-time was 2 h when the sample was set still in a flow bench subject to minimal vibrations from the fan.

For the final sample processing procedure, 0.65 mL of the NTA resin was added to 1 L samples, which are pH 1.7 to 2, and samples were shaken vigorously on a shaker table for 2 h. Under these conditions, $67 \pm 4\%$ of the Fe is removed with each extraction. All samples were extracted twice using the same batch method for a total extraction efficiency of about 89%. Because recovery is not quantitative, it is important to know what is the isotope effect of Fe binding to the resin. To check this, samples were prepared by adding 20 nM IRMM-014 Fe in Fe-free seawater, and about 20% of this Fe was extracted onto 50 µL of resin. The δ^{56}Fe values of two samples prepared in this fashion were −0.02‰ and −0.04‰, well within typical analytical error. Isotopic fractionation between resin-bound and dissolved Fe is not an important source of error in this method. Resin was separated from the seawater by filtration in a PFA filter apparatus with a 47 mm filter holder (Savillex) with a 1.0 µm polycarbonate membrane (Whatman). Fe was eluted from the NTA resin in the same filter holder with 8 mL of 1.2 N HCl (Fig. 1B).

Chemical blanks were determined for resin which had been intitially cleaned by leaching for 1 week in 1% HCl, and had been in continuous use in pH 2 seawater for several months. The chemical blank for extraction onto the NTA resin was evaluated by performing an extraction on 1 L Fe-free seawater, made Fe-free by multiple extractions with the NTA resin. The blank was found to be 1.1 ± 0.6 ng Fe (1σ SD, $n = 9$), after further purification by anion exchange chromatography.

2.4. Sample purification

After the initial extraction from seawater using the NTA resin, samples were further purified by anion exchange chromatography. While NTA may bind strongly to many cations, Fe can be efficiently separated from these cations by conversion to $FeCl_4^-$ in strong HCl and

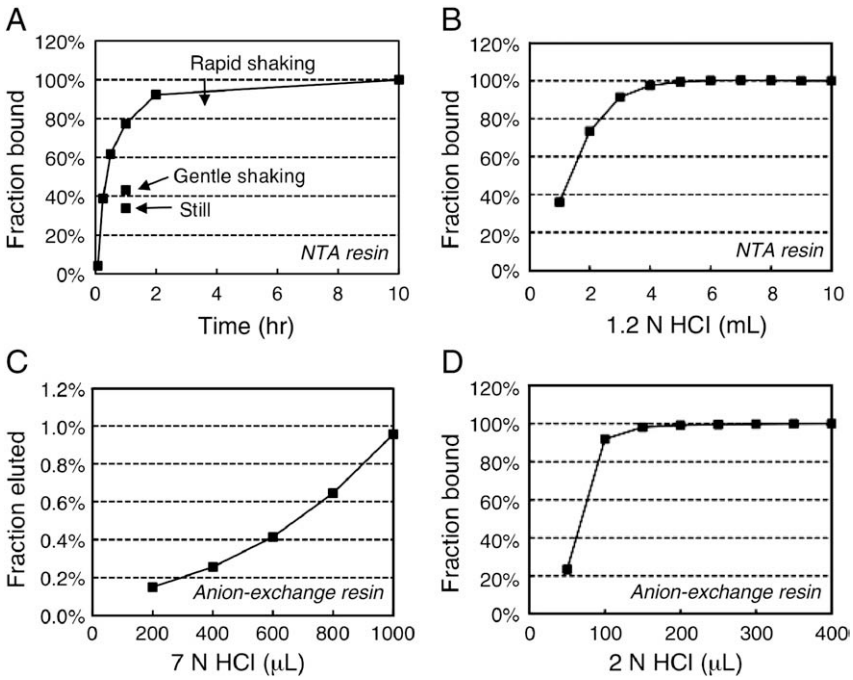

Fig. 1. Iron uptake and elution curves for both of the resins used to extract and purify Fe from seawater. The half-time for Fe uptake onto the extraction resin from pH 2 seawater, normalized to uptake at 10 h, is 0.5 h when samples are shaken quickly, about 1.5 h when shaken very slowly, and about 2 h if samples are sitting still (A). Elution of Fe from 0.65 mL of the NTA resin is 100% complete after the addition of ~6 mL 1.2 N HCl (B). Premature elution of Fe from the anion exchange resin during rinsing with 7 N HCl increases from 0.2% to 1.0% for 200 to 1000 µL of rinse. (C). Elution of Fe from the purification column is complete (100%) after the addition of 250 µL 2 N HCl (D). The timescale for Fe unbinding from the NTA resin in 10% HCl is less than 10 s.

purification by anion exchange (Strelow, 1980). While this method has successfully been used to purify Fe from many types of samples for isotope analysis, the typical blanks for these resins are 20 ng of Fe per mL of resin and typical methods use 1 to 2 mL of resin (e.g. Beard and Johnson, 1999; Dauphas et al., 2004). Such high blanks would swamp the small amounts of Fe in seawater. In order to decrease the blank, procedures were developed to purify Fe on very small columns containing only 20 µL of resin. Columns were fashioned from 0.313″ ID 4:1 heatshrink PTFE for a final column diameter of 2 mm and a height of 4.5 mm. Frits were fashioned from polyethylene frit material cut with a clean razor blade. Columns were leached in 10% HCl to remove Fe contamination before use. Because the distribution coefficient is higher for resins with a higher degree of crosslinking, macroporous AG-MP1 resin (Biorad) was used. Elution profiles were tested by adding 1 µg of Fe to these columns dissolved in 50 µL of 7 N HCl + 0.001% H_2O_2. The possibility of premature elution of the Fe from the columns was tested by rinsing the column with 50 µL aliquots of 7 N HCl + 0.001% H_2O_2 up to a total volume of 1 mL. Only 0.65% of the Fe was eluted in the first 800 µL (Fig. 1C), suggesting that premature elution is not a problem even with such small columns. The elution of Fe in 50 µL aliquots of 2 N HCl was rapid, with 100% recovery of the Fe within the first 250 µL (Fig. 1D). Blanks for these small purification columns were 0.3 ± 0.2 ng Fe (1σ SD, $n = 7$).

The final optimized procedure was to load samples onto the column dissolved in 200 to 500 µL 7 N HCl, to rinse with 300 µL 7 N HCl + 0.001% H_2O_2, and to elute in 400 µL 2 N HCl. Samples were evaporated to remove HCl and dissolved in 0.07 N HNO_3 for isotopic analysis.

2.5. Isotopic analyses

2.5.1. Instrumental setup

Isotopic analyses were performed on a Neptune multi-collector ICPMS (Thermo Scientific). Because the amount of Fe in seawater is small, every opportunity was taken to increase instrumental sensitivity. An 'x'-type skimmer cone is used to increase ion transmission at the front end. Samples were introduced via an Apex-Q (ESI) desolvating inlet system with 70 µL min^{-1} teflon nebulizer. However, the optional Apex desolvating membrane was not used because it did not greatly increase sensitivity while it decreased signal stability. Samples were measured in a high-resolution mode to separate interferences such as the abundant argide polyatomics ArO^+ and ArN^+ (e.g. Weyer and Schwieters, 2003). The Neptune is equipped with a moveable slit tongue so that two high-resolution modes are available, termed 'high' and 'medium' in the software. The slit width in 'high' and 'medium' resolution can change depending on the dimensions of the slit installed. Over the course of this project, most samples were analyzed in 'medium' resolution through a 32 µm slit or in 'high' resolution through a 25 µm slit. After burning though a 'medium' resolution slit, a few samples with particularly high Fe concentrations were measured in 'high' resolution with a 16 µm slit. We found that a 'medium' resolution 50 µm slit was too wide to accurately measure δ^{56}Fe. By visual inspection, the Fe beams appeared to produce flat-topped peak shoulders which were fully separated from polyatomic interferences. However, internal errors in the ^{56}Fe/^{54}Fe isotope ratio were much higher than would have been predicted for an interference-free beam, suggesting that there was tailing of the polyatomic interference beams into the flat-topped region of the Fe beams.

2.5.2. Correction for isobaric interferences

Signal intensity was measured at masses 52, 53, 54, 56, 57, 58, and 60. The abundance of ^{52}Cr and ^{53}Cr was used to correct for Cr interference at mass 54. All samples were spiked with 500 ppb Ni in order to monitor changes in instrumental mass bias using ^{58}Ni and ^{60}Ni. With multiple isotopes at mass 54 (^{54}Cr and ^{54}Fe) and 58 (^{58}Fe and ^{58}Ni), an iterative solution can be used to solve the Cr correction on Fe, the Fe correction on Ni, and the Ni instrumental mass bias correction on Cr. Corrections were performed in the following order: 1) Ni (uncorrected for the ^{58}Fe interference) is used to calculate instrumental mass bias β_1 2) β_1 is used to correct for the ^{54}Cr interference and calculate the signal for ^{54}Fe 3) the ^{56}Fe/^{54}Fe ratio is used to calculate β_2 for Fe which includes the effects of instrumental mass bias, 4) β_2 is used to calculate the ^{58}Fe interference at mass 58, and 5) the corrected ^{60}Ni/^{58}Ni ratio is used to monitor instrumental mass bias. Errors are minimized by performing corrections in this order because our samples have high Ni/Fe and high Fe/Cr ratios. Therefore, a single run through the correction procedure outlined above is sufficient to optimize all corrections and there is no benefit to performing multiple iterations of this procedure.

2.5.3. Mass bias correction

Cu, Ni, and Fe double-spike may all be used to correct for instrumental mass bias in Fe isotope analysis, typically in conjunction with sample-standard bracketing (Dauphas et al., 2009, and references therein). However, there are disadvantages to each of these methods. Because the mass dispersion on a Neptune is insufficient to simultaneously measure masses from 52 to 65, mass bias correction with Cu requires measurement in dynamic mode (e.g. Arnold et al., 2004). This roughly doubles the analysis time for each sample without increasing the time Fe isotopes are measured, effectively decreasing sensitivity by a factor of ~2 which can be detrimental when only small amounts of Fe are available for analysis. Using an Fe double-spike makes it impossible to monitor for isobaric interferences. A linear relationship in a double-isotope plot (e.g. δ^{56}Fe versus δ^{57}Fe) is a good check for the absence of isobaric interferences, but a double spike produces only a single isotope ratio.

There is anecdotal evidence that Ni does not work well for correcting large variations in instrumental mass bias. However, we use Ni to monitor instrumental mass bias but not to actually correct the final δ^{56}Fe measurements. Mass bias corrections are made only by sample-standard bracketing. Two pieces of evidence suggest that there is no sample-specific mass bias that needs to be corrected. $\delta^{60}Ni_{sample\text{-}standard}$ values for all seawater samples were evenly distributed around zero, showing that there was not a systematic change in instrumental mass bias for samples compared to standards. Also, the standard deviation of $\delta^{60}Ni_{sample\text{-}standard}$ values for all seawater samples was 0.036‰, similar to 0.042‰ for pure-metal standards, demonstrating that our purification scheme was sufficient to remove all contaminants.

2.5.4. Modification of Faraday cup resistors

Even in the absence of an ion beam, Faraday cup detectors record a noisy background voltage due to Johnson noise (also Johnson-Nyquist noise or thermal noise), caused primarily by thermal noise in the high-ohmic resistors contained in the amplifier feedback loop. Johnson noise was determined by recording the voltages on each collector when the analyzer gate valve was closed so that no ions could make it through to the back end of the instrument (Fig. 2).

Two of the amplifiers on the Neptune at Caltech have been modified to use 10^{12} Ω resistors which decreases the effect of Johnson noise but does not eliminate it. Johnson noise was measured for each of our Faraday cups and each of our amplifiers, including the two amplifiers with 10^{12} Ω resistors (Fig. 2). Compared to the average Johnson noise with 10^{11} Ω resistors, we find a 34%–39% decrease in Johnson noise with 10^{12} Ω resistors. This is slightly less than the 50% decrease in noise observed by Wieser and Schwieters (2005), and is less than the theoretical maximum $\sqrt{10}$-fold (68%) reduction in noise that would be possible if the resistor were the only source of impedance in the feedback circuit.

While the use of 10^{12} Ω resistors actually increases the voltage in the amplifier circuit by an order of magnitude compared to 10^{11} Ω

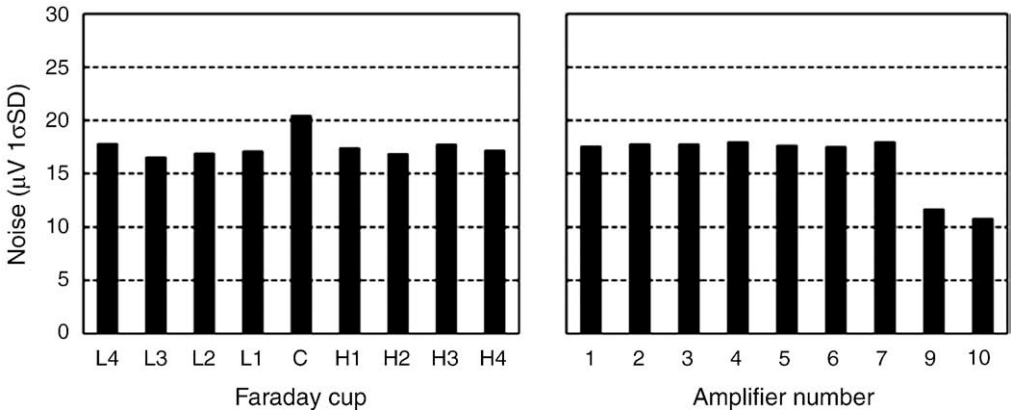

Fig. 2. The magnitude of Johnson noise varies for different cups and for different amplifiers. The mean standard deviation in Johnson noise is plotted here for one thousand 4.194 s integrations, presented as the mean values of the noise (1σ S.D.) for each cup over all nine amplifiers, and the mean noise for each amplifier over each 9 cups. Amplifiers 9 and 10 have 10^{12} Ω resistors, which decreases Johnson noise by about 35% compared to 10^{11} W resistors. Johnson noise also varies between cups, with about a maximum 15% difference in the magnitude of Johnson noise on some cups compared to others (e.g. cup H1 compared to cup C).

resistors, the Neptune reports voltages normalized to the voltage that would be expected with 10^{11} W resistors. The maximum reported-voltage that can be measured with 10^{12} Ω resistors is therefore 5 V, compared to a maximum of 50 V with 10^{11} Ω resistors. For analysis of all the seawater samples, the 10^{12} Ω resistors were used for the cups collecting masses 54 and 56 in order to minimize the amount of Johnson noise on these detectors. 10^{11} Ω resistors were used for all detectors for analysis of samples with higher amounts of Fe (>100 ppb) so that the maximum voltage on mass 56 was not exceeded. Johnson noise is unimportant as a source of error at such high Fe concentrations (Section 3.1.2), so the use of 10^{11} Ω resistors does not affect analytical precision.

2.5.5. Optimizing analytical integration period

In order to choose the optimal length of time for analyzing our samples, we have investigated the timescale of instrumental mass bias drift. While sample-standard bracketing can correct for any liner drift in instrumental mass bias, it will not correct for non-linear drift. We measured a single Fe standard many times over the course of several hours to evaluate the effects of non-linear drift. By calculating δ^{56}Fe when a "sample" 56/54 ratio was corrected using the 56/54 ratios measured directly before and afterwards as bracketing standards, and comparing this with δ^{56}Fe values calculated for "sample" ratios with bracketing standards run as much as 180 min beforehand and afterwards, we could evaluate the timescale for both linear and non-linear instrumental mass bias drift.

An 800 ppb solution of standard Fe (~34 V on mass 56) was run over the course of several hours and signal intensities were measured in 4.2 s integration periods. After applying the correction for isobaric interferences, ^{56}Fe/^{54}Fe ratios were calculated for each integration period. Data points were discarded if they were more than two standard deviations away from the mean of the ten ratios collected before and after. We then calculated δ^{56}Fe ratios for each of these integration periods, using for bracketing standards the integration periods that were between 1 min and 180 min before and after the sample. We found that there was no significant non-linearity (>0.01‰) in instrumental mass bias drift on timescales of less than about one or two hours (Fig. 3). Of course, this does not mean that the total instrumental mass bias drift is so small. The total drift in instrumental mass bias over 120 min was 0.5‰, but the deviation from linearity over this same period was less than 0.01‰.

For the final analytical procedure, 58 cycles of data were collected for 4.2 s each. Because data collection began as soon as the sample probe entered the solution, the first 8 cycles were discarded to account for sample uptake and signal stabilization. Cycles for which the 56/54 ratio was more than 2.5 standard deviations from the mean were discarded, which was usually zero cycles and very rarely more than two cycles. The final analytical time for each standard and sample was therefore about 3.5 min. Standard-sample-standard groups were run back-to-back, with no washout between standards and samples. Between each group we rinsed with clean 0.5% HNO_3 for about 10 min, then measured a 0.5% HNO_3 blank for on-peak zero correction. Running each sample in a group with two standards allowed us to match standard concentrations individually to each sample. It also decreases the Johnson noise error in the blank by $\sqrt{2}$ because the same blank is used for both bracketing standards and the sample.

3. Analysis of error

Measuring iron isotopes on the very small quantities of Fe that can be extracted from seawater presents a unique set of challenges and requires a thorough understanding of the sources of error. In this section, several different sources of error are considered. First, the internal error for a single ~3.5 min analysis of a single sample is considered. Second, intermediate error for multiple analyses of the same purified Fe sample is considered. Finally, external error is

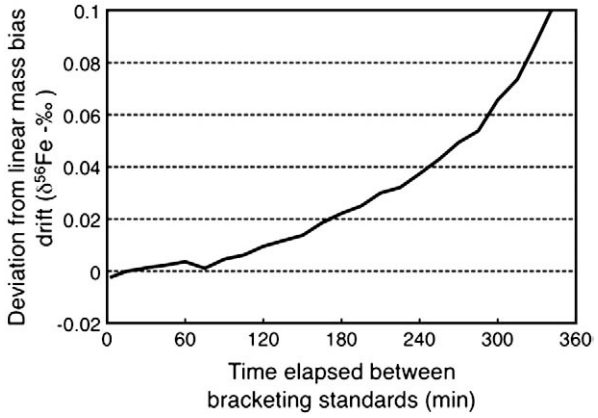

Fig. 3. The error in δ^{56}Fe due to nonlinear drift in instrumental mass bias increases as the spacing between samples and standards increases. Because typical methods for mass-bias correction assume linearity in the drift of instrumental mass bias (e.g. by sample-standard bracketing with two standards on either side), curvature in the instrumental mass bias drift may lead to errors in the standard-corrected δ^{56}Fe. We find that these errors are minimal when the total time elapsed from beginning analysis of the first bracketing standard to finishing analysis of the second standard is less than about 60 min. This is equivalent to analysis of each standard and the sample for a maximum of 20 min, assuming that instrumental blanks are not measured between standards and samples.

considered when 1 L aliquots of the original seawater are extracted and purified separately for isotopic analysis. The blank error caused by Fe contamination introduced during sample collection, processing, or analysis is also discussed. From this analysis of error, we can predict the precision with which δ^{56}Fe can be measured for different concentrations of Fe in seawater.

By analyzing the different sources of error in detail, it is also possible learn which analytical strategies are most effective at increasing the precision and accuracy of δ^{56}Fe measurements. Quantifying internal, intermediate, and external error allows us to evaluate the costs and benefits of running samples in a more concentrated or more diluted form and the benefit of performing multiple analyses. The only way to reduce the effect of intermediate error is to perform multiple analyses of each sample, and the only way to reduce external error is to extract and purify Fe from different aliquots of the same seawater multiple times. However, there are disadvantages to performing such multiple extractions and/or multiple analyses as well. Additional time and effort are involved in repeating chemistry and analysis. Multiple chemical extractions may increase the blank error. Increasing the number of analyses on sample with a limited amount of Fe requires diluting the sample, which decreases the error due to mass bias flicker but increases the error due to Johnson noise (Section 3.1). By quantifying various sources of error, we can learn which analytical strategies are most effective for measuring seawater δ^{56}Fe.

3.1. Internal error

Each individual analysis of a sample or standard takes about 3.5 min, over which time approximately fifty usable data "cycles" are recorded. Signal intensity is recorded at each mass and, after correction for isobaric interferences (Section 2.5.2) the internal standard deviation and standard error for the ^{56}Fe/^{54}Fe ratio over these cycles is calculated. Three distinct processes which contribute to the total observed internal error have been identified: counting statistics, Johnson noise, and a third processes which we believe is probably rapid flicker in instrumental mass bias (Fig. 4).

3.1.1. Counting statistics

Counting statistics, sometimes referred to as 'shot noise', set a theoretical limit on the analytical precision which can be achieved for a given number of ions counted. Counting statistics describe the uncertainty inherent in approximating a continuous quantity such as signal intensity (e.g. counts per time) by measuring a finite number of individual events that are randomly distributed in time, such as ion detections at the Faraday cup. In order to calculate the impact of counting statistics on internal error, one must first calculate the total number of ions collected at each mass. This is done by taking the average voltage over the integration period and using the conversion of $6.25 \cdot 10^7$ cps V^{-1} to convert from voltage to the number of individual ions collected (n). The counting statistics error in n for a single isotope is set by the standard deviation of the Poisson distribution

$$\sigma_n = \sqrt{n} \tag{2}$$

Following the basic rules of error propagation, the error in an isotope ratio R is

$$\sigma_R = \sqrt{\frac{\sigma_a^2}{a^2} + \frac{\sigma_b^a}{b^2}} \tag{3}$$

where a and b are the signal intensity of each isotope and σ_a and σ_b are the errors in those quantities. If the quantity of each isotope is expressed as the number of counts, then the internal error due to counting statistics is

$$\sigma_{\text{Counting statistics}} = \sqrt{\frac{n_a + n_b}{n_a \cdot n_b}} \tag{4}$$

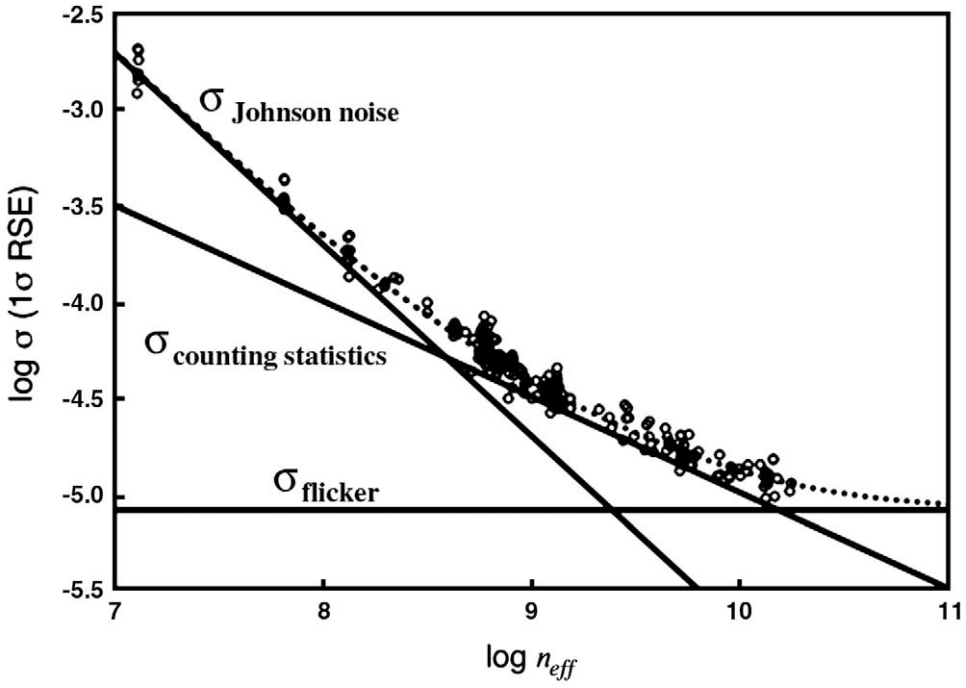

Fig. 4. The errors (1σ RSE) in ^{56}Fe/^{54}Fe for 252 measurements of samples or standards are calculated from the variability in ^{56}Fe/^{54}Fe ratios of ~54 consecutive 4.2 s cycles of data. Signal intensity is given as the effective number of counts collected over this period (n_{eff}) (Eq. (5)). The error due to counting statistics is based on theoretical calculations (Eq. (7)) (slope = −1/2). The error due to Johnson noise is calculated based on independent measurements of Johnson noise on each of the detectors (Eq. (13)) (slope = −1). The other source of error, which we believe may be caused by flicker in the instrumental mass bias is calculated by assuming a constant error and adjusting the magnitude of σ_{other} so that the predicted total error best matches the observed errors in the ratio using a least-squares fit. The total internal error for a single sample combines the effects of all three individual sources of error (Eq. (16)) (dashed line).

where n_a and n_b are the number of counts recorded for isotopes a and b, respectively. We define a new quantity for the effective number of counts (n_{eff})

$$n_{\text{eff}} = \frac{n_a \cdot n_b}{n_a + n_b} \tag{5}$$

so that in analogy to Eq. (2)

$$\sigma_{n_{\text{eff}}} = \sqrt{n_{\text{eff}}} \tag{6}$$

The relative error in the isotope ratio due to counting statistics can then be given as

$$\sigma_{\text{Counting statistics}} = \frac{1}{\sqrt{n_{\text{eff}}}} \tag{7}$$

so that, in a logarithmic plot, there is a linear relationship between $\sigma_{\text{counting statistics}}$ and n_{eff} with a slope of −0.5 (Fig. 4). By using n_{eff} as our proxy for signal intensity, instead of the number of counts for either of the individual isotopes, our plot of counting statistics error intercepts the origin just as the error in n intercepts the origin when plotted against n.

3.1.2. Johnson noise

Johnson noise (Section 2.5.3) also contributes to the error in our measurements of isotopes. The effect of Johnson noise is observed as a fluctuation in the background voltage recorded by Faraday cups in the absence of an ion beam. The effect of Johnson noise on the precision with which an ion beam signal can be measured is determined by the error in voltage

$$V_{\text{measured}} = V_{\text{signal}} \pm V_{\text{Johnson noise}} \tag{8}$$

where V_{measured} is the recorded voltage, V_{signal} is the voltage due to the ion beam captured in the Faraday cup, and V_{Johnson} is the magnitude (standard error) of the baseline Johnson noise. To determine the Johnson noise error in an isotope ratio we can use Eq. (3), and find that

$$\sigma_{\text{Johnson noise}} = \sqrt{\left(\frac{V_{\text{Johnson noise } a}}{V_a}\right)^2 + \left(\frac{V_{\text{Johnson noise } b}}{V_b}\right)^2} \tag{9}$$

If R is the ratio of the two isotope being analyzed

$$R = V_a / V_b \tag{10}$$

then we can combine Eqs. (9) and (10) to get

$$\sigma_{\text{Johnson noise}} = \frac{R}{V_a}\sqrt{\left(\frac{V_{\text{Johnson noise } a}}{R}\right)^2 + V^2_{\text{Johnson noise } b}} \tag{11}$$

In order to compare the effects of Johnson noise to the effects of counting statistics error, voltage can be expressed in terms of the number of counts (n) using the conversion of $6.25 \cdot 10^7$ cps V^{-1} for 10^{11} Ω resistors, and substituting in the quantity n_{eff}

$$\sigma_{\text{Johnson noise}} = \frac{R}{n_{\text{eff}}(R+1)}\sqrt{\left(\frac{n_{\text{noise } a}}{R}\right)^2 + n^2_{\text{noise } b}} \tag{12}$$

and the logarithmic relationship between $\sigma_{\text{Johnson noise}}$ and n_{eff} can be defined as

$$\log\left(\sigma_{\text{Johnson noise}}\right) = -\log(n_{\text{eff}}) + \log\left(\frac{R}{(R+1)}\sqrt{\left(\frac{n_{\text{noise } a}}{R}\right)^2 + n^2_{\text{noise } b}}\right) \tag{13}$$

In a logarithmic plot, the error in isotope ratio measurements due to Johnson noise has a linear relationship to signal intensity (n_{eff}) with a slope of −1 and an intercept that is calculated with R, $n_{\text{noise a}}$, and $n_{\text{noise b}}$ (Fig. 4). For our measurements of Fe isotopes on the Neptune using 10^{12} Ω resistors, the intercept is 4.29. This is equivalent to Johnson noise with a standard deviation of 11 μV for 4.194 s integration periods.

3.1.3. Other error

The combined effects of counting statistics and Johnson noise account for much of our observed internal error (Fig. 4). However, at the highest signal intensities ($\log n_{\text{eff}} > 9.5$) we can see that the internal error is greater than predicted by the combination of Johnson noise and counting statistics alone. We therefore suggest there must be a third contribution to internal error, which we hypothesize as caused by short-timescale variability in instrumental mass bias due to 'flicker' in the plasma conditions (σ_{flicker}). Andren et al. (2004) have identified mass bias instability during ion extraction from the plasma as a significant source of error in multi-collector ICP-MS. Their measurements of boron isotopes deposited on sample and skimmer cones demonstrated that there is significant isotopic fractionation as the ion beam passes between these two cones. Changing plasma position by moving the torch or adjusting gas flows was observed to have a large impact on the extent of instrumental mass bias for many elements. Based on these findings, they conclude that rapid fluctuations in plasma conditions are an important source of error in isotope ratio analysis. This short timescale variability in instrumental mass bias would be independent of signal intensity. We quantify σ_{flicker} as independent of signal intensity and adjust the magnitude so that the total predicted error best matches the observed error by a least-squares fit. The magnitude of this error is determined to be $10^{-5.09}$ which is equivalent to 0.0081‰ in δ^{56}Fe. (Fig. 4).

3.1.4. Total internal error

The three sources of error discussed above, $\sigma_{\text{counting statistics}}$, $\sigma_{\text{Johnson noise}}$ and σ_{flicker} all contribute to the total observed error in the measurement of a single isotope ratio. The error in a single ratio is

$$\sigma^2_{\text{unbracketed}} = \sigma^2_{\text{counting statistics}} + \sigma^2_{\text{Johnson noise}} + \sigma^2_{\text{flicker}} \tag{14}$$

Because sample-standard bracketing is used to correct for drift in instrumental mass bias, it is also necessary to account for the error δ^{56}Fe for the two bracketing standards. The δ^{56}Fe value of a sample is corrected for drift in instrumental mass bias by comparing the measured isotope ratio to the isotope ratio for standards measured both before and after the sample:

$$\delta^{56}Fe = \left(\frac{R_{\text{Unbracketed sample}}}{{}^1/_2\left(R_{\text{sample before}} + R_{\text{sample after}}\right)} - 1\right) \cdot 1000 \tag{15}$$

where R is the ratio of ^{56}Fe/^{54}Fe. Assuming that the signal intensity is the same for samples and standards, the internal error for any single analysis of a sample or standard will be equal, and the total internal error of a standard-bracketed sample is

$$\sigma_{\text{internal}} = \sqrt{\frac{3}{2}}\sigma_{\text{unbracketed}}. \tag{16}$$

3.2. External and intermediate error

Quantifying internal error is only the first step towards predicting the true precision with which we can measure seawater δ^{56}Fe. Internal error sets a lower limit on the overall error of our measurements, but other sources of error must also be taken into account. For the purposes of this paper, we discuss three types of error and refer to them as 'internal', 'intermediate', and 'external'. Internal error (σ_{internal}), as discussed above, is the error for a single ~3.5 min analysis of a sample corrected for instrumental mass bias with two bracketing standards. Intermediate error ($\sigma_{\text{intermediate}}$) is the error between several different analyses of the same sample solution (e.g. the same autosampler vial) over different analytical runs. Transition-metal stable isotope data are typically reported along with the intermediate error calculated from ~2–4 repeat analyses of each sample. The total intermediate error ($\sigma_{\text{intermediate-total}}$) combines the effects of internal error and any intermediate error that is expressed during the longer time-frame between repeat analyses. Others have termed this "$\sigma_{\text{mass spectrometric}}$" or "$\sigma_{\text{MassSpec}}$" (Dauphas et al., 2009; Humayun and Clayton, 1995). Total external error ($\sigma_{\text{external-total}}$) is the best estimate of the accuracy with which we are measuring true seawater δ^{56}Fe. Total external error includes the effects of internal error, intermediate error, and any additional error that derives from the process of extracting and purifying Fe from seawater. External error is estimated by comparing δ^{56}Fe of 1 L aliquots taken from the same original carboy of seawater which are run through the entire purification and analysis process separately.

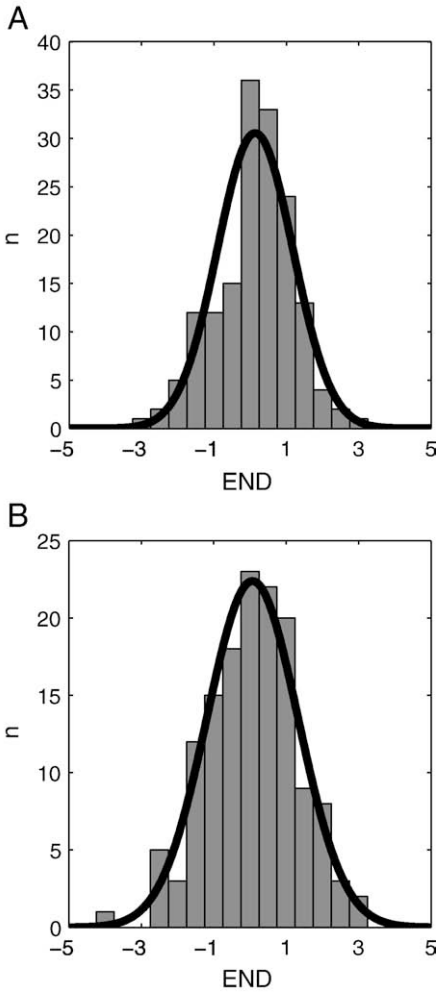

Fig. 5. Histograms of the error-normalized deviates (END) for 160 pairs of intermediate replicates (A) and 141 pairs of external replicates (B) compared to a Gaussian distribution. The variance of END is 1.04 for intermediate replicates when calculated with internal error, suggesting that 4% of the total intermediate error is due to internal error. The standard deviation of the END distribution for external replicates is 1.26, indicating that 79% of the total external error comes just from the internal analytical error.

3.2.1. Intermediate error

The total intermediate error is the error for repeat analyses of an individual concentrated and purified sample. Typically, a concentrated and purified sample is stored in a single sample vial and is analyzed multiple times during a single analytical session or during different analytical sessions so that the error for multiple analyses is the intermediate error. This total intermediate error is itself the combination of internal error with any intermediate sources of error that manifest themselves only between analyses or during different analytical sessions so that

$$\sigma_{\text{intermediate-total}} = \sqrt{\sigma^2_{\text{internal}} + \sigma^2_{\text{intermediate}}} \tag{17}$$

Because many of our samples have been analyzed multiple times, it is possible to compare the internal error for these analyses with the intermediate error. Overall, there were 160 data pairs in this study for which samples were measured during two different analytical sessions. For each of these pairs, error normalized deviates can be calculated as:

$$END = \frac{R_1 - R_2}{\sqrt{\sigma_1^2 + \sigma_2^2}} \tag{18}$$

where R_1 and R_2 are the measured isotopic ratios for two analyses and σ_1 and σ_2 are the absolute errors associated with these ratios. If values of R are normally distributed with a variance σ^2, the error-normalized deviates for multiple pairs of data will also be normally distributed with a standard deviation of 1. Calculating the error-normalized deviates using σ_{internal} yields an END distribution with a standard deviation of 1.04 (Fig. 5A). Because there is no obvious relationship between END and signal intensity (Fig. 6A), we assume that $\sigma_{\text{intermediate}}$ scales with σ_{internal} and calculate that $\sigma_{\text{intermediate-total}}/\sigma_{\text{internal}}$ is also 1.04. Thus, the variability between repeat analyses of a single sample is due almost entirely to internal error.

3.2.2. External error

The total external error reflects the combined effects of internal error and any external error that arises during Fe extraction and purification procedures by

$$\sigma_{\text{external-total}} = \sqrt{\sigma^2_{\text{internal}} + \sigma^2_{\text{external}}} \tag{19}$$

As above (Section 3.2.1), the magnitude of external error can be estimated from the distribution of error-normalized deviates for 141 external isotope ratio pairs. ENDs are calculated for separate analyses of two different samples produced by separately extracting and purifying 1 L aliquots of the same original seawater sample. The standard deviation of the END distribution calculated using internal errors is 1.26, meaning that the total external error is 26% greater than would be predicted if internal error were the only source of error (Fig. 5B). The variance in END values does not correlate with signal intensity, suggesting that the relative magnitudes of external error and internal error are constant regardless of sample Fe concentration (Fig. 6B).

3.3. Blank error

With picomolar to nanomolar concentrations of Fe in seawater compared to the ~5% crustal abundance of Fe, it can be quite difficult to keep samples free of contaminate Fe. For example, a single 1 μg dust particle with typical Fe crustal abundance would contain between 4

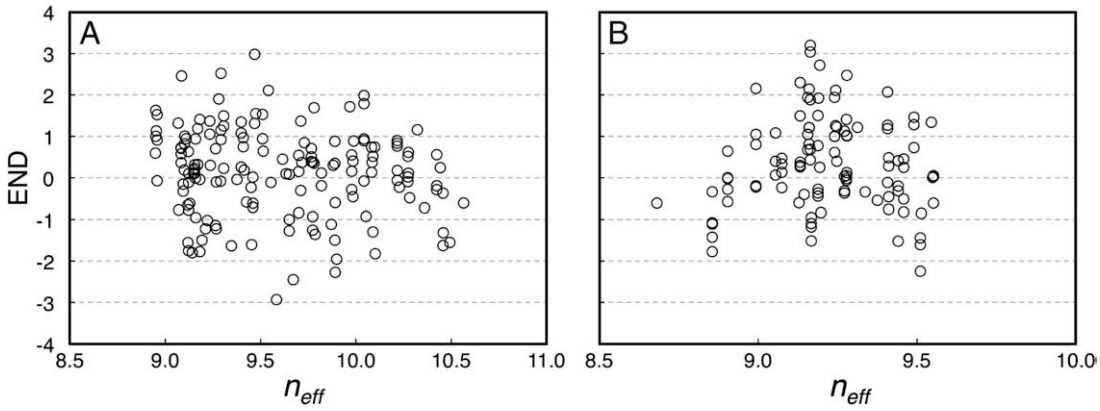

Fig. 6. Error-normalized deviates were calculated for intermediate pairs of replicates (A) and external pairs of replicates (B) and in both cases we find that there is not a strong relationship between signal intensity (n_{eff}) and ENDs. This suggests that the processes that give rise to intermediate and external errors are not correlated with signal intensity.

and 100 times as much Fe as a typical liter of seawater. The effect of Fe contamination on our measurement of δ^{56}Fe depends on the amount of contamination and the isotope composition of both the seawater and the contaminant:

$$\delta^{56}Fe_{sample} = \delta^{56}Fe_{seawater} \cdot f_{seawater} + \delta^{56}Fe_{contaminant} \cdot f_{contaminant} \quad (20)$$

where $\delta^{56}Fe_{sample}$ is the iron isotope composition of the contaminated sample, $\delta^{56}Fe_{seawater}$ is the iron isotope composition of the original seawater, $\delta^{56}Fe_{contaminant}$ is the isotope composition of the contaminating Fe, $f_{seawater}$ is the fraction of Fe in the sample that was in the original seawater, and $f_{contaminant}$ is the fraction of Fe in the sample from contamination. Thus, the influence of blank on sample δ^{56}Fe value increases both with increasing amounts of contamination and with greater offsets between the δ^{56}Fe of seawater and contaminant Fe. Assuming that the $\delta^{56}Fe_{contaminant} = 0$, similar to the crustal average δ^{56}Fe, and knowing that levels of Fe contamination for our process are 1.1 ng (Section 2.3), it is possible to calculate the probable impact of contamination on measured seawater δ^{56}Fe at a range of concentrations (Table 2). For most samples, the contribution of blank would alter the δ^{56}Fe by less than 0.05‰, which is less than typical analytical error for the samples which we have analyzed so far. The effect of contamination is greatest for a sample in the surface waters of the San Pedro Basin where Fe concentrations are very low (0.3 nM) and the δ^{56}Fe is substantially offset from continental values (−0.97‰).

Table 2
Effect of procedural blank on measured seawater δ^{56}Fe. Representative sample Fe concentrations and δ^{56}Fe values are chosen from seawater samples we have analyzed from the North Atlantic near Bermuda and the San Pedro Basin. The error caused by a 1.1 ng blank with $\delta^{56}Fe_{contamination} = 0$‰ is compared with the predicted analytical error for the same sample. Blank errors are generally smaller than the external analytical error except for samples with very low Fe concentrations and very positive or very negative δ^{56}Fe.

Sample description	Depth (m)	[Fe] (nM)	δ^{56}Fe (‰)	Blank error (‰)	2σ external analytical error (‰)
North Atlantic Fe minimum	75	0.3	0.30	0.02	0.09
North Atlantic Fe maximum	1500	0.9	0.35	0.01	0.06
North Atlantic δ^{56}Fe maximum	2500	0.7	0.71	0.02	0.07
Deep San Pedro Basin	895	7.7	−1.82	0.00	0.03
San Pedro Basin Fe minimum	35	0.3	−0.97	0.06	0.09

3.4. Optimal strategies for measuring seawater δ^{56}Fe

3.4.1. Maximizing sensitivity

Because error increases with decreasing sensitivity (n_{eff}), maximizing sensitivity is an important component of our overall strategy to reducing analytical error. Several modifications have been made to our instrument to increase sensitivity. We use an x-type skimmer cone which increases ion transmission at the front end and typically increases Fe sensitivity by 200% to 300%, depending on the particular set of cones used and tuning conditions of the day. The disadvantage of using x-cones is that more frequent replacement of the high/medium- and low-resolution slits may be required. X-cones increase the transmission of all ions, including abundant species such as Ar+ which are most responsible for wear on the slits. Samples are introduced via an Apex-Q sample introduction system which increases sensitivity compared to a traditional cyclonic spray chambers. The Apex-Q has a heated spray chamber which decreases the loss of sample by condensation on the spray-chamber walls, followed by a cooling loop which helps to remove moisture from the gas flow. With the Apex-Q, our sensitivity was 0.042 ± .003 V ppb^{-1} (1σ SD) for ^{56}Fe over several analytical sessions in "high" resolution mode with a 25 μm slit. This is a 3.5-fold increase in sensitivity compared to typical sensitivities achieved with a Scott cyclonic spray chamber.

Future developments that further increase sensitivity will lead to further decreases in error. One possible approach is to optimize the slit width specifically for analysis of Fe isotopes. We have found that it is possible to accurately measure δ^{56}Fe with slits as wide as 32 μm, leading to a mass resolution (m/Δm of the peak side 5% to 95% peak height) of 9500. However, we were unable to accurately measure Fe isotopes using a 50 μm slit (m/Δm = 6020). An intermediate slit width might be found at which sensitivity is maximized while the resolution necessary to separate interferences is maintained. Also, the sensitivity might be increased by using an autosampler that allows the entire sample to be analyzed. In our current configuration with a CETAC ASX-100 autosampler, measurements stop at the time the autosampler probe is withdrawn from the sample. It would be possible to continue analysis after this point with a different autosampler, and even to take up the entire sample until air is aspirated.

3.4.2. Minimizing internal error

Internal error is dominated by different processes depending on the signal intensity (or concentration) of the sample being analyzed (Fig. 7). When samples are run at very low concentrations (<10 ppb), internal error is dominated by Johnson noise. At very high

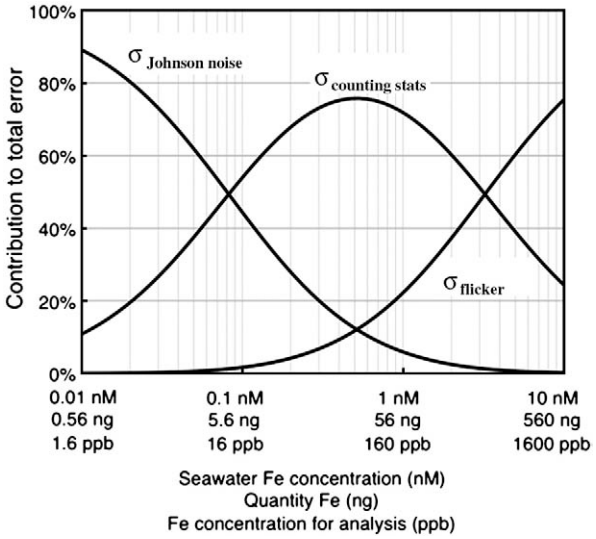

Fig. 7. The fraction of internal error due to Johnson noise, counting statistics, and mass bias changes depending on the signal intensity. Signal intensity is given as the concentration of Fe in a 1 L seawater sample, the total weight of iron per sample, and the concentration of iron in a purified 350 μL sample for analysis. For small amounts of sample, error is dominated by Johnson noise which is most effectively reduced by running samples at the highest possible concentration for a short period of time. For large amounts of sample, error is dominated by $\sigma_{flicker}$, which can be minimized by running samples for as long as possible, even if is necessary to dilute the samples. Counting statistics error is independent of the sample concentration and the length of analysis.

concentrations (>1000 ppb), internal error is dominated by mass bias flicker. In between, error is dominated by counting statistics. This is an important finding because different strategies can be used to minimize these different sources of error. Specifically, the magnitude of different sources of error will vary depending on whether a given quantity of sample is run for a short time period in a very concentrated solution or if it is run for a longer time in a more dilute solution.

Of the three sources of internal error, only counting statistics is independent of sample dilution. Because counting statistics error depends only on the total number of counts (n) (Eq. (2)), it does not matter whether these counts are collected over a short period of time from a concentrated solution or over a longer period of time from a more dilute solution.

The best way to minimize the Johnson noise error is to run the sample at the highest concentration possible, maximizing the ratio of V_{signal} to $V_{Johnson\ noise}$ (Eq. (9)). The signal voltage is inversely proportional to the integration time of the measurement (t), while the magnitude of Johnson noise is inversely proportional to $\sqrt{t}$. The Johnson noise error depends on the ratio $V_{Johnson\ noise}/V_{signal}$ and therefore

$$\sigma_{Jonhson\ noise} \propto \sqrt{t} \tag{21}$$

Mass-bias flicker error is independent of signal intensity, but by increasing the analysis time we can decrease the mass bias standard error by

$$\sigma_{flicker} \propto \frac{1}{\sqrt{t}} \tag{22}$$

Diluting samples to increase the total amount of time over which a sample can be analyzed is therefore an effective strategy for minimizing internal error due to mass bias.

There are practical limits on how much one can change sample dilution to minimize internal error. Minimum analysis times are determined mostly by the length of the "wash-in" period between the first introduction of a sample into the inlet system and the stabilization of the isotope ratios. With our Apex, for example, it typically takes about 30 to 35 s after the first detection of a new sample for the sample concentration to increase to a stable value and for the isotope ratio to stabilize. Since this sample is not useful for analysis, it is reasonable to use a total sample analysis time of at least a few minutes. Sample may also be wasted if there is leftover liquid in the nebulizer uptake tube or the bottom of the vial after analysis. It may therefore be wise to optimize sample volume to the calculated uptake rate, or to continue analysis after aspiration of the complete sample in order to make sure that none is wasted. Regardless of all the factors mentioned above, diluting a sample in order to perform replicate analyses will increase the impact of Johnson noise. Therefore, we recommend analyzing each seawater iron isotope sample only once in a small volume.

3.4.3. The benefit of multiple purifications

With measurements of the contributions of internal and external error, it is possible to calculate the relative benefit of processing and purifying a seawater sample in several separate aliquots, rather than processing the same volume of seawater in a single aliquot. If samples are processed in k separate aliquots, for example several one-liter samples are separately extracted and purified from the same original seawater carboy, the error in our measurement of the seawater δ^{56}Fe will be reduced by

$$\sigma_{separate} = \frac{\sigma_{external-total}}{\sqrt{k}} \tag{23}$$

If the same k liters of seawater were combined in a single aliquot, and the resulting sample was diluted to a larger volume so that the sample could be measured more times, the contribution of the internal error would be reduced while the magnitude of the external error would be the same as for a 1 L aliquot

$$\sigma_{combined} = \sqrt{\left(\frac{\sigma_{internal}}{\sqrt{k}}\right)^2 + \sigma^2_{external}} \tag{24}$$

Combining Eqs. (23), (24), and substituting with

$$\Phi = \frac{\sigma_{external-total}}{\sigma_{internal}} \tag{25}$$

yields

$$\frac{\sigma_{separate}}{\sigma_{combibed}} = \frac{\Phi}{\sqrt{1 + k(\Phi^2 - 1)}} \tag{26}$$

For Φ equal to 1.26 (Section 3.2.2), and k equal to 3, $\sigma_{separate}/\sigma_{combined}$ is 0.76. That is, processing the same quantity of seawater in three separate batches rather than in one single aliquot is expected to reduce the total external error by 24%. Of course, if a single aliquot of seawater is divided into multiple portions, and each portion is purified and analyzed separately, this may increase the blank error. Therefore, we do not recommend multiple, separate purifications for seawater iron isotope samples.

3.4.4. Choosing an optimized procedure

The various analytical procedures discussed above each have different effects on analytical error (Fig. 8). We must balance the costs and benefits of these various permutations in order to choose an optimal strategy for analysis of seawater δ^{56}Fe. For seawater with Fe concentrations between 0.1 nM and 10 nM, we suggest that the Fe should be extracted from 1 L aliquots of seawater, that the entire quantity of extracted Fe should be measured for Fe isotopes in a single ~2–4 min analysis, that amplifiers with 10^{12} Ω resistors are not

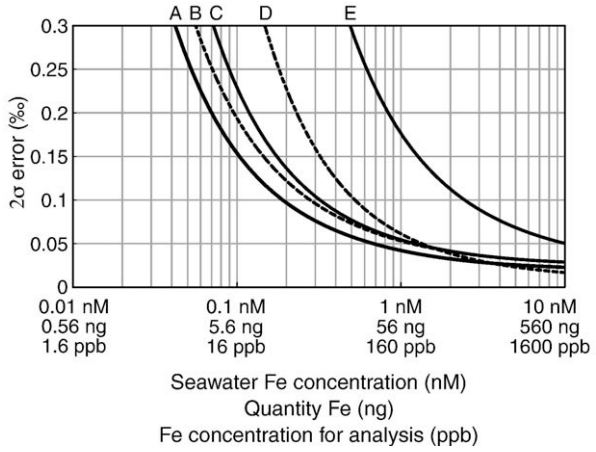

Fig. 8. Analytical error can be predicted as a function of Fe concentration. The analytical error in δ^{56}Fe (2σ RSE) is plotted as a function of signal intensity as represented by the concentration of Fe in 1 L seawater needed to extract the given amount of Fe, the total amount of Fe per sample and the concentration of Fe in a 350 µL sample for analysis. Errors curves shown are, from left to right at the top of the figure, internal error (A), external error under optimized analytical conditions (Eq. (27)) (B), external error if measurements are made using 10^{11} Ω resistors instead of 10^{12} Ω resistors (C), external error if samples are diluted by a factor of ten and analyzed for ten times as long, instead of as a more concentrated single sample (D), and external error without using an x-type skimmer and Apex-Q to increase signal intensity (E). The optimal conditions for analysis depend on sample concentration. Increasing sensitivity reduces error at all Fe concentrations. Diluting samples and increasing analytical time reduces the error from mass bias flicker, but increases the error due to Johnson noise, so that dilution decreases external error for high-Fe samples but increases error for low-Fe samples, thus the crossover between line D and others at ~1 nM Fe. The benefit of 10^{12} Ω resistors is seen only at lower Fe concentrations where error is dominated by Johnson noise.

critical but that they be used for measurement of ^{56}Fe and ^{54}Fe if available, and that an inlet system be used which maximizes signal intensity. One liter quantities of seawater should contain enough Fe for accurate discrimination of natural variability in seawater δ^{56}Fe (Fig. 8). The benefit of extracting Fe from larger quantities of seawater (>1 L) is offset by the proportional increase in blank, and the internal analytical error for small amounts of Fe can be addressed by increasing the sample concentration during analysis to swamp the effects of Johnson noise. The benefit of measuring Fe isotopes during a single analysis is that the sample can be run in a more concentrated form. This will increase the analytical error due to plasma flicker, but decreases the analytical error due to Johnson noise (Section 3.4.2). With the small amounts of Fe present in seawater, Johnson noise is the dominant source of error (Figs. 7, 8). It is a lucky coincidence that the same procedures designed to minimize error, extraction of Fe from a single liter of seawater and a single analysis of the extracted Fe, also reduce the time necessary to measure seawater δ^{56}Fe. This will make analysis of seawater δ^{56}Fe possible even for large-scale efforts such as GEOTRACES where hundreds of samples may be collected and analyzed.

Using this procedure, the total external error in δ^{56}Fe for analysis of a 1 L seawater sample is predicted as a function of seawater Fe concentration (nM) by:

$$\sigma = 1.54\sqrt{\left(10^{-\log\left(10^{9.67}[\mathrm{Fe}]\right)} + 4.29\right)^2 + \left(10^{-0.5\log\left(10^{9.67}[\mathrm{Fe}]\right)}\right)^2 + 0.0000081^2} \quad (27)$$

This predicted error was compared with actual δ^{56}Fe values measured for process standards, which were created by adding IRMM-014 to Fe-free seawater and extracting the Fe for analysis alongside samples six times over several months. δ^{56}Fe values for these standards are generally equal to zero within the predicted error, confirming that these error estimates are realistic (Fig. 9).

4. Conclusions

We have developed chemical procedures to extract iron from seawater for isotopic analysis, and optimized methods for measurement of δ^{56}Fe by ICP-MS. We employ bulk extraction of Fe from seawater with an NTA-resin, and use miniaturized columns for anion exchange chromatography. This method has sufficiently high recovery (89%), low blank (1.1 ± 0.6 ng Fe), and no isotopic fractionation during processing, so it is possible to measure δ^{56}Fe on 1 L samples of natural seawater. Extensive error analysis clarifies what are the sources of error in measuring seawater δ^{56}Fe, and what strategies are most effective at minimizing error.

Internal error for a single Fe isotope analysis can be described as the combination of Johnson noise error, counting statistics error, and plasma flicker error. These sources of error should be common to any ICP-MS analysis and the total error for measurement of an isotope ratio can therefore be described by

$$\sigma = \sqrt{\left(10^{-\log(n_{\mathrm{eff}}) + x}\right)^2 + 10^{-0.5\log(n_{\mathrm{eff}})})^2 + y^2} \quad (28)$$

where n_{eff} is a measurement of signal intensity and the three terms under the square root represent the three sources of error, with x being a constant which depends on the magnitude of Johnson noise, and y being a constant which depends on the magnitude of flicker in instrumental mass bias. Because each of these sources of error scales differently with n_{eff}, we find that the best error-minimization strategies change depending on the amount of sample available. A surprising finding is that, for very small samples, error is minimized by running the sample as concentrated as possible because internal error is dominated by Johnson noise at low signal intensities. While conventional wisdom in mass spectrometry is that more analyses and longer analyses lead to better precision, this is true only for higher signal intensities where mass bias flicker is the dominant source of error.

For measurements of δ^{56}Fe in seawater, internal error was found to dominate the overall error in our measurements, compared to intermediate error and external error. The relative magnitudes of these errors was determined by comparing internal errors with the intermediate error, observed for multiple analyses of the sample during different analytical sessions, and external error observed for samples which had been prepared by separately extracting and purifying Fe from the same original carboy of seawater. Of the total error for measurements of seawater δ^{56}Fe, we found that 79% was due to internal error, 4% was due to the intermediate, and 17% of the error was due to external error. Interestingly, while the conventional practice in isotope geochemistry is to report the intermediate error (e.g., standard deviation of several replicates of a single sample) we

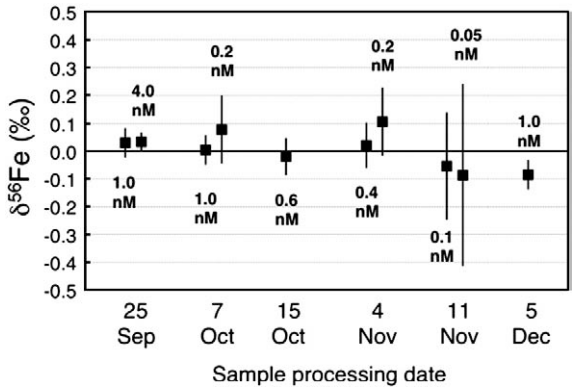

Fig. 9. Standards prepared by adding a known amount of IRMM-014 Fe to Fe-free seawater were processed and analyzed alongside samples. The measured δ^{56}Fe values are plotted along with the predicted external error based on sample concentration. The concentration of Fe added to seawater is marked above or below the data points.

find that this is the least valuable sort of error to report. Intermediate error is almost completely determined by internal error, but internal error can be estimated much more accurately than intermediate error because a large number of cycles go into a single internal error calculation, while intermediate error is typically estimated from just a handful of replicate analyses. Based on our exploration of the different sources of error, we propose that the best strategy for analysis of seawater δ^{56}Fe is to extract Fe from 1 L seawater samples and to measure to entire quantity of extracted Fe during a single short analysis, in order to minimize Johnson noise error. With these methods it is possible to measure seawater δ^{56}Fe with sufficient accuracy to discover natural variability and with sufficient ease to make large-scale sampling efforts possible.

References

Andren, H., Rodushkin, I., Stenberg, A., Malinovsky, D., Baxter, D.C., 2004. Sources of mass bias and isotope ratio variation in multicollector ICP-MS: optimization of instrumental parameters based on experimental observations. Journal of Analytical Atomic Spectrometry 19 (9), 1217–1224.

Arnold, G.L., Weyer, S., Anbar, A.D., 2004. Fe isotope variations in natural materials measured using high mass resolution multiple collector ICPMS. Analytical Chemistry 76 (2), 322–327.

Beard, B.L., Johnson, C.M., 1999. High precision iron isotope measurements of terrestrial and lunar materials. Geochimica Et Cosmochimica Acta 63 (11–12), 1653–1660.

Beard, B.L., et al., 1999. Iron isotope biosignatures. Science 285 (5435), 1889–1892.

Beard, B.L., Johnson, C.M., Von Damm, K.L., Poulson, R.L., 2003. Iron isotope constraints on Fe cycling and mass balance in oxygenated Earth oceans. Geology 31 (7), 629–632.

Bergquist, B.A., Boyle, E.A., 2006. Iron isotopes in the Amazon River system: weathering and transport signatures. Earth and Planetary Science Letters 248 (1–2), 54–68.

Brantley, S.L., et al., 2004. Fe isotopic fractionation during mineral dissolution with and without bacteria. Geochimica Et Cosmochimica Acta 68 (15), 3189–3204.

Bullen, T.D., White, A.F., Childs, C.W., Vivit, D.V., Schulz, M.S., 2001. Demonstration of significant abiotic iron isotope fractionation in nature. Geology 29 (8), 699–702.

Croal, L.R., Johnson, C.M., Beard, B.L., Newman, D.K., 2004. Iron isotope fractionation by Fe(II)-oxidizing photoautotrophic bacteria. Geochimica Et Cosmochimica Acta 68 (6), 1227–1242.

Crosby, H.A., Johnson, C.M., Roden, E.E., Beard, B.L., 2005. Coupled Fe(II)-Fe(III) electron and atom exchange as a mechanism for Fe isotope fractionation during dissimilatory iron oxide reduction. Environmental Science & Technology 39 (17), 6698–6704.

Crosby, H.A., Roden, E.E., Johnson, C.M., Beard, B.L., 2007. The mechanisms of iron isotope fractionation produced during dissimilatory Fe(III) reduction by Shewanella putrefaciens and Geobacter sulfurreducens. Geobiology 5 (2), 169–189.

Dauphas, N., Rouxel, O., 2006. Mass spectrometry and natural variations of iron isotopes. Mass Spectrometry Reviews 25 (4), 515–550.

Dauphas, N., et al., 2004. Chromatographic separation and multicollection-ICPMS analysis of iron. Investigating mass-dependent and -independent isotope effects. Analytical Chemistry 76 (19), 5855–5863.

Dauphas, N., Pourmand, A., Teng, F.-Z., 2009. Routine isotopic analysis of iron by HR-MC-ICPMS: how precise and how accurate? Chemical Geology 267 (3–4), 175–184.

de Jong, J., et al., 2007. Precise measurement of Fe isotopes in marine samples by multi-collector inductively coupled plasma mass spectrometry (MC-ICP-MS). Analytica Chimica Acta 589 (1), 105–119.

Escoube, R., Rouxel, O.J., Sholkovitz, E., Donard, O.F.X., 2009. Iron isotope systematics in estuaries: the case of North River, Massachusetts (USA). Geochimica Et Cosmochimica Acta 73, 4045–4059.

Fantle, M.S., DePaolo, D.J., 2004. Iron isotopic fractionation during continental weathering. Earth and Planetary Science Letters 228 (3–4), 547–562.

Humayun, M., Clayton, R.N., 1995. Precise determination of the isotopic composition of potassium — application to terrestrial rocks and lunar soils. Geochimica Et Cosmochimica Acta 59 (10), 2115–2130.

Lacan, F., et al., 2008. Measurement of the isotopic composition of dissolved iron in the open ocean. Geophysical Research Letters 35 (24).

Lohan, M.C., Aguilar-Islas, A.M., Franks, R.P., Bruland, K.W., 2005. Determination of iron and copper in seawater at pH 1.7 with a new commercially available chelating resin, NTA Superflow. Analytica Chimica Acta 530 (1), 121–129.

Lohan, M.C., Aguilar-Islas, A.M., Bruland, K.W., 2006. Direct determination of iron in acidified (pH 1.7) seawater samples by flow injection analysis with catalytic spectrophotometric detection: application and intercomparison. Limnology and Oceanography-Methods 4, 164–171.

Rouxel, O., Shanks, W.C., Bach, W., Edwards, K.J., 2008a. Integrated Fe- and S-isotope study of seafloor hydrothermal vents at East Pacific rise 9–10°N. Chemical Geology 252 (3–4), 214–227.

Rouxel, O., Sholkovitz, E., Charette, M., Edwards, K.J., 2008b. Iron isotope fractionation in subterranean estuaries. Geochimica Et Cosmochimica Acta 72 (14), 3413–3430.

Severmann, S., et al., 2004. The effect of plume processes on the Fe isotope composition of hydrothermally derived Fe in the deep ocean as inferred from the Rainbow vent site, Mid-Atlantic Ridge, 36 degrees 14′ N. Earth and Planetary Science Letters 225 (1–2), 63–76.

Severmann, S., Johnson, C.M., Beard, B.L., McManus, J., 2006. The effect of early diagenesis on the Fe isotope compositions of porewaters and authigenic minerals in continental margin sediments. Geochimica Et Cosmochimica Acta 70 (8), 2006–2022.

Sharma, M., Polizzotto, M., Anbar, A.D., 2001. Iron isotopes in hot springs along the Juan de Fuca Ridge. Earth and Planetary Science Letters 194 (1–2), 39–51.

Staubwasser, M., von Blanckenburg, F., Schoenberg, R., 2006. Iron isotopes in the early marine diagenetic iron cycle. Geology 34 (8), 629–632.

Strelow, F.W.E., 1980. Improved separation of iron from copper and other elements by anion-exchange chromatography on a 4-percent cross-linked resin with high-concentrations of hydrochloric-acid. Talanta 27 (9), 727–732.

Weyer, S., Schwieters, J., 2003. High precision Fe isotope measurements with high mass resolution MC-ICPMS. International Journal of Mass Spectrometry 226 (3), 355–368.

Wieser, M.E., Schwieters, J.B., 2005. The development of multiple collector mass spectrometry for isotope ratio measurements. International Journal of Mass Spectrometry 242 (2–3), 97–115.